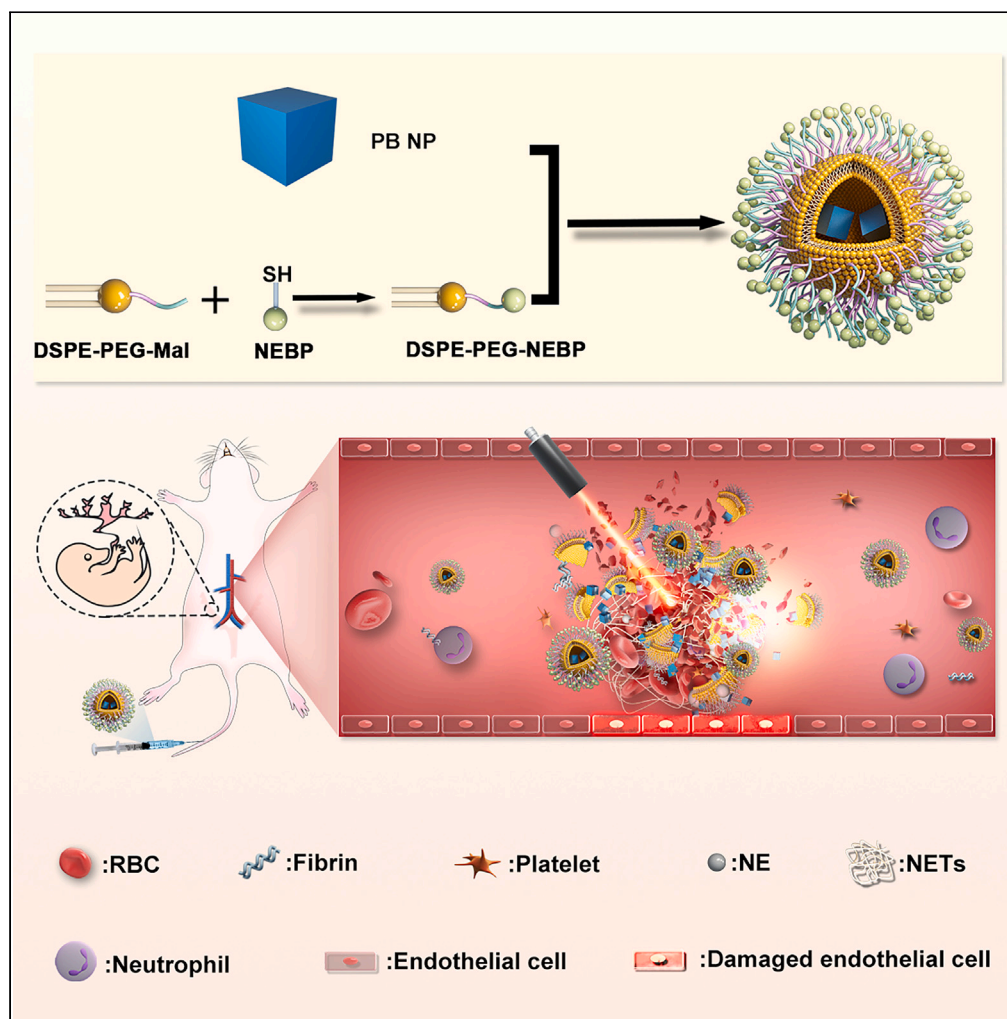**CellPress**
OPEN ACCESS

Article

NET-targeted nanoparticles for antithrombotic therapy in pregnancy

Yijie Zhou, Lin Xu, Pingsong Jin, Na Li, Xuehai Chen, Anyu Yang, Hongbo Qi

cxh5256@gmail.com (X.C.)
babyboboann_yay@163.com (A.Y.)
qihongbocy@gmail.com (H.Q.)

Highlights

This study focuses on the development of versatile nanoparticles modified with a neutrophil elastase-binding peptide surface, allowing for specific targeting of NET both *in vitro* and *in vivo*

The combination of antioxidant activity from PB-NEBP liposomes with photothermal therapy effects shows promise in achieving comprehensive antithrombotic treatment by enabling thrombolysis, scavenging of ROS, and reduction of inflammatory factors

This non-invasive thrombolysis approach is deemed safe for both the mother and fetus, making it a viable strategy for managing pregnancy-related diseases

Article

NET-targeted nanoparticles for antithrombotic therapy in pregnancy

Yijie Zhou,[1,3,5,6,7] Lin Xu,[1,3,5,6,7] Pingsong Jin,[2,3,7] Na Li,[1,3,6] Xuehai Chen,[1,3,8,*] Anyu Yang,[6,*] and Hongbo Qi[2,3,4,*]

SUMMARY

Pulmonary embolism caused by deep vein thrombosis (DVT) is a major contributor to maternal morbidity and mortality. There is still an unmet need for safe and effective treatment options for DVT during pregnancy. Recent research has shown that neutrophil extracellular trap (NET) formation plays a very vital role in thrombosis. We created nanoparticles surface-modified by neutrophil elastase (NE)-binding peptide that can target activated neutrophils specifically *in vitro* and *in vivo*. Prussian blue nanoparticles (PB NPs) designed in the core scavenges abnormally elevated reactive oxygen species (ROS) in the vascular microenvironment and acts as a photothermal agent to mediate photothermal therapy (PTT) to damage fibrin network structure. Based on the data we have included, this noninvasive therapeutic approach is considered safe for both mothers and the fetus. Furthermore, our findings indicate that this therapeutic approach has a significant alleviation effect on intrauterine growth restriction caused by maternal thrombosis.

INTRODUCTION

Deep vein thrombosis (DVT) occurring in pregnancy substantially contributes to pulmonary embolism and several pregnancy-related disorders, including pathological alterations within placental tissues, intrauterine growth restriction, and preeclampsia. These complications are tightly linked to life-threatening issues and adverse outcomes during pregnancy.[1] The heightened hypercoagulable state induced by physiological changes during pregnancy is posited as an evolutionary protective mechanism. It serves to prevent women from the risk of bleeding during miscarriage and childbirth. However, it also designates pregnancy as a robust risk factor for DVT.[2–4] Presently, upon the confirmation of DVT, the essential therapeutic measures involve the prescription of anticoagulation, to manage symptomatic expression, impede the advancement of thrombotic phenomena, and significantly reduce the likelihood of post-thrombotic syndrome, as well as the consequential ramifications of pulmonary embolism.[5,6] Direct oral anticoagulants (DOACs) stand as the favored therapeutic approach for DVT due to their demonstrated efficacy, heightened safety profile, and superior convenience when compared with warfarin. However,[6] DOACs should be avoided in pregnancy due to the lack of established safety and efficacy data. Antiplatelet drugs and thrombolytic agents increase the risk of fetal congenital malformation and maternal bleeding.[7–10] While low-molecular-weight heparin (LMWH) is often recommended for the treatment of pregnancy-associated DVT,[11] it is important to consider the potential risks involved. Subcutaneous injections of LMWH may lead to skin reactions and inflammation, and there is also a risk of hemorrhage and osteoporotic fractures. Therefore, developing innovative and safe treatment strategies for DVT in pregnancy remains a challenge.

Since the discovery of neutrophil extracellular trap (NET) formation and release in 2004,[12] NET has commanded interdisciplinary attention. Recent research shows that NET acts as a determinate in DVT, suggesting that uncontrolled and excessive NET formation in vasculature potentially leads to pathological thrombotic disorders.[13] Neutrophils, the primary responders at injury sites, are pivotal in these processes.[14] In human venous thrombus samples, especially during organizing stages, NETs are notably abundant.[15] These extracellular traps play a pivotal role in promoting vessel occlusion by serving as scaffold, for procoagulant molecules, platelets, and red blood cells. NET components also actively advance coagulation via intrinsic or extrinsic pathways.[13] Considering these discoveries, the inhibition of NETs has been proposed as a promising antithrombotic strategy.[16] The main components of NETs are DNA, histones, and neutrophil elastase (NE).[17] We

[1]Department of Obstetrics, The First Affiliated Hospital of Chongqing Medical University, Chongqing 400016, China
[2]Department of Obstetrics and Gynecology, Women and Children's Hospital of Chongqing Medical University, Chongqing 401147, China
[3]Chongqing Key Laboratory of Maternal and Fetal Medicine, Chongqing Medical University, Chongqing 400016, China
[4]Joint International Research Laboratory of Reproduction and Development of Chinese Ministry of Education, Chongqing Medical University, Chongqing 400016, China
[5]Department of Department of Reproductive Medicine, Guiyang Maternal and Child Health Care Hospital, Guiyang 550003, China
[6]Institute of Ultrasound Imaging, the Second Affiliated Hospital of Chongqing Medical University, Chongqing 400010, China
[7]These authors contributed equally
[8]Lead contact
*Correspondence: cxh5256@gmail.com (X.C.), babyboboann_yay@163.com (A.Y.), qihongbocy@gmail.com (H.Q.)
https://doi.org/10.1016/j.isci.2024.109823

pay special attention to NE because it has been observed to disrupt both fibrinolysis and clotting, constituting approximately one-third of the cytosolic proteins observed in NETs.[18] NE is exclusively present on neutrophils but not on other leukocyte subsets. More importantly, it is only exposed on the surface of neutrophils during cell activation.[19,20] The high biocompatibility, non-toxicity, and controllable drug distribution make liposomes an attractive option for drug delivery vehicles. Therefore, we developed NET-specific liposomes attached to the lipid shell of NE-binding peptide (NEBP) to target NEs on NETs.

As extensively discussed in recent scholarly works, a wealth of studies has underscored the intricate regulation of both thrombus formation and resolution by reactive oxygen species (ROS). The processes of DVT formation and resolution are influenced by the nuanced influence of ROS, which exert their effects on proteolysis, complement system, fibrinolysis, and coagulation. Furthermore, ROS intricately modulate various effector cells, including endothelial cells, erythrocytes, neutrophils, fibroblasts, platelets, monocytes, and mast cells. Pathways leading to NET release comprise the signaling induced by ROS, which are phagocyte NADPH homolog NOX2-generated. Expressed in both plasma and phagosome membranes,[21] NOX2 is activated by a spectrum of stimuli, inclusive of lipopolysaccharide, proinflammatory cytokines, Toll-like receptor agonists, and chemical agents (inclusive of phorbol 12-myristate 13-acetate [PMA]), triggering NET formation as well. In the context of thrombo-inflammation, NOX2 intricately plays a regulatory role in platelet-neutrophil interactions by influencing the functionality of surface receptors,[22] which potentially serves as an indirect facilitator of NETosis. In light of these insights, the inhibition of NETs/neutrophils has been proposed as a promising antithrombotic strategy. As an inorganic nanomaterial, Prussian blue (PB) has garnered attention due to its robust antioxidant activities.[23,24] Its utility as a light absorber, coupled with exceptional photothermal conversion efficiency, mediated by the Landau damping effect mediated by near-infrared (NIR),[25,26] positions PB as a potential non-pharmacological intervention for thrombotic diseases.

Inspired by PB and the active thrombus-targeting property of NETs, we conceived a holistic antithrombotic therapeutic strategy that amalgamates non-pharmaceutical thrombolysis, photothermal therapy (PTT), and ROS scavenging to achieve a synergistic and potent antithrombotic effect. In this investigation, PB-NEBP liposomes were synthesized to form a PB nanoparticle (NP)-loaded nanocore, NEBP, which was linked to the surface of the liposomes. After intravenous injection, PB-NEBP liposomes effectively target the NET structure in venous thrombi; NIR accelerated PB NPs release into thrombus site. PB NPs regulate ROS in the thrombus microenvironment to inhibit and reduce the formation of NETs in the thrombus and mitigate associated inflammatory factors, such as tumor necrosis factor alpha (TNF-α) and interleukin-6 (IL-6), to the greatest extent. Besides, PTT has an efficient therapeutic effect for thrombolytic treatment. Moreover, safety assessments have shown that this treatment is safe for both mothers and offspring, highlighting its potential as a promising therapeutic nanomedicine for managing thrombotic disorders during pregnancy.

RESULTS

Characteristics and stability of the liposomes

PB NPs were synthesized and their physical characteristics were observed, the nanoparticles appeared in the form of a dark blue suspension. Transmission electron microscopy analysis revealed that the PB NPs were cubic shapes (Figure 1A). Furthermore, X-ray diffraction analysis (Figure 1B) of PB NPs confirmed that we successfully synthesized PB NPs. Particle size analysis results indicated that the mean diameter of the PB NPs was 56 ± 6.0 nm. The zeta potential of PB NPs was -8.75 mV (Figure 1E). The UV spectrophotometric diagram showed that the absorption peak of PB NPs was approximately 702 nm (Figure 1H),[27] which was the typical UV absorption peak of PB NPs. The absorption spectrum of PB NPs in the UV-visible range displayed concentration-dependent absorption patterns, particularly in the NIR I region spanning from 700 to 900 nm. Notably, a distinct peak in absorption was observed within this range, which served as a crucial indicator of NIR-mediated PTT.

Mass spectrometry analysis (MS) of NEBP showed that the synthetic molecular weight was 1470.40 Da (Figure S1), which was basically consistent with the theoretical molecular weight, indicating that NEBP was successfully synthesized. The peptide purity was >95% as ascertained by high-performance liquid chromatography (Figure S2). Meanwhile, the successful conjugation of DSPE-PEG-NEBP was confirmed by MS (Figure S3). After being dissolved in double-distilled water, the PB-NEBP liposomes nanocomplex appeared as a blue emulsion, which slightly stratifies when left to stand. As observed under a light microscope, the PB-NEBP liposomes nanocomplex was spherical, with a smooth surface. The diameters of the PB liposomes and PB-NEBP liposomes were 140 ± 1.5 (Figure 1C) and 146 ± 3.0 nm (Figure 1D), respectively. The polydispersity index values for all the nanoformulations were found to be below 0.3, suggesting a tightly controlled particle size distribution. The zeta potentials of the PB liposomes and PB-NEBP liposomes were -16.05 and -24.57 mV (Figure 1E). Upon incubation in phosphate-buffered saline (PBS) (Figure 1F) or PBS enriched with 10% fetal bovine serum (Figure 1G), we observed no obvious difference or change in particle size within 7 days, indicating that the components in the serum have no significant impact on the material, and the material also has good stability under neutral conditions. In order to confirm the successful encapsulation of PB NPs, the absorption spectrum of PB-NEBP liposomes was examined (Figure 1H). This absorption peak of PB NPs was consistent with the absorption peak of PB-NEBP-targeting nanocomplexes. The absorption peak observed in the PB NPs spectrum was also present in the PB-NEBP liposomes, reinforcing the notion of efficient encapsulation. It is worth noting that the loading efficiency of PB NPs within the PB-NEBP liposomes was found to be 69%, which further attests to the successful encapsulation process. This finding holds significant implications for future investigations involving PTT and modulation of the thrombus microenvironment.
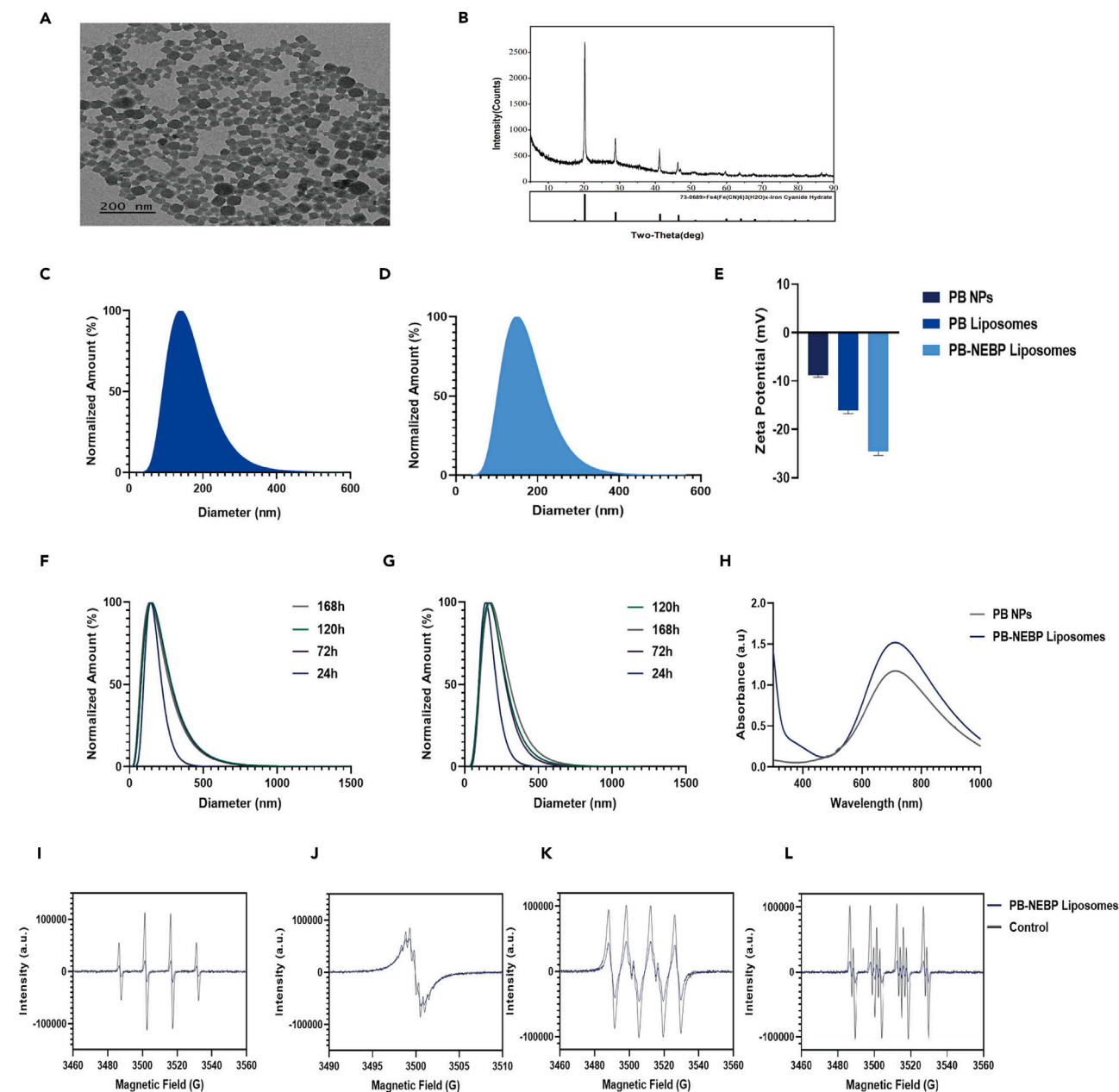
Figure 1. Characterization of PB-NEBP liposomes and antioxidant enzymatic activity *in vitro*

(A) TEM image of PB NPs.

(B) XRD analysis of PB NPs.

(C and D) The size distribution of PB liposomes and PB-NEBP liposomes.

(E) Zeta potentials of PB NPs, PB Liposomes, and PB-NEBP liposomes.

(F and G) Changes in the mean diameter of PB-NEBP liposomes after incubation with PBS or FBS for predetermined time periods.

(H) The corresponding absorbance intensity of PB NPs and PB-NEBP liposomes.

(I-L) Elimination of Hydroxyl radicals (I), hydrogen peroxide (J), superoxide radicals (K), and peroxyl radicals (L) by PB-NEBP liposomes.

In vitro antioxidant activity of PB-NEBP liposomes

PB-NEBP liposomes effectively eliminated the scavenging ability of hydroxyl radicals, hydrogen peroxide, superoxide radicals, and peroxyl radicals (Figures 1I–1L). These results indicated that PB-NEBP liposomes were capable of eliminating a broad spectrum of ROS. The ROS-scavenging capability of PB-NEBP liposomes was mainly contributed by PB NPs.[23] This is in line with the previous finding that PB NPs are superoxide dismutase-mimetic agents capable of eliminating ROS.

Photothermal performance and PB NPs release *in vitro*

After PB-NEBP liposomes of different concentrations were irradiated by a laser (1.2 W/cm^2), it can be seen that the temperature of each group increased to varying degrees, showing a positive correlation trend between rising temperature and the concentration of nanocomposites (Figure 2A). After 1 mg/mL PB-NEBP liposomes were irradiated by a laser with different powers, the temperature increased to varying degrees, showing a trend of positive correlation between rising temperature and laser power (Figure 2B). After 1 mg/mL PB-NEBP liposomes were irradiated by three cycles of laser switching (1.2 W/cm^2), the temperature increased with the same trend, and no obvious temperature peak decrease was observed (Figure 2C). The results of this experiment show that PB-NEBP liposomes have good photothermal conversion ability. The results indicate that the PB NPs in the PB-NEBP liposomes nanocomposite have absorbed NIR light that can be converted into heat. The nanocomposite formed by wrapping PB NPs with the liposomes shell still has good photothermal conversion ability. PB-NEBP liposomes showed a stable temperature rise and fall under three cycles of laser switching, demonstrating good photothermal conversion characteristics and photothermal stability. The aforementioned *in vitro* photothermal property results all show that PB-NEBP liposomes can be used as good photothermal substances. Controlled sustained release and targeted release of drugs in drug delivery systems can be triggered by many physical and chemical stimuli in the microenvironment, such as light, heat, magnetism, and pH.[28,29] Under laser irradiation, the *in vitro* release rate of PB NPs in PB-NEBP liposomes was significantly higher than that in the nonirradiated group at same time point (Figure 2D). This may be because after laser irradiation, the PB-NEBP liposomes generate heat, which accelerates the degradation rate of the polymer and accelerates the release of PB NPs. Moreover, the laser irradiated the thrombus site to target the release of the PB NPs at the thrombus site. In this experiment, the prepared PB-NEBP liposomes had a high drug-loading capacity. Therefore, the PB-NEBP liposomes can be used as a multifunctional drug delivery system that can achieve controlled and sustained release of drugs.

Targeting and inhibiting effects on NETs

Human peripheral blood neutrophils were isolated and purified using the reference method, and the cell purity was 84% (Figure 2E), as measured by flow cytometry. The following experiments were performed using isolated and purified human peripheral blood neutrophils. One of the main ways that NETs promote thrombosis is to provide a scaffold for the adhesion of platelets and red blood cells.[29,30] The formation of this stent is not only the structural basis for thrombosis, but many components on the stent can also actively activate the coagulation process. Neutrophils release NETs after activation. This form of NET formation is induced by a variety of NOX-dependent proinflammatory substances, including IL-8, TNF, and some drugs, such as PMA. The one with the strongest induction ability is PMA.[31,32] We used PB-NEBP liposomes and NEBP liposomes to coculture with PMA-activated neutrophils. Compared with the NEBP liposomes and PBS groups, the number of NETs formed in the PB-NEBP liposomes coculture group was reduced (Figure 2G). The SEM experimental results show that compared with the PBS group, simply adding PMA can activate neutrophils to release NETs, adding PB-NEBP liposomes can reduce PMA-mediated neutrophil activation (Figure 2H). After different interventions, it was suggested that PB-NEBP liposomes can reduce the area of NETs released by neutrophils (Figure 2F).

Effect of targeting activated neutrophils *in vitro*

The main components of NETs are DNA histones and NE.[15] NE accounts for one-third of the cytosolic proteins found in NETs and has been shown to interfere with both clotting and fibrinolysis.[33] NE is only exposed on the surface of neutrophils during cell activation.[34] To target NE on activated neutrophils, we created multifunctional nanoparticles surface-modified by a 14 amino acid peptide (CGEAIPMSIPPEVK) termed NEBP that binds to NE.[35] Confocal laser microscopy was used to observe the accumulation of PB-NEBP liposomes and blank liposomes in NETs (Figure 3A). Anti-histone 3 (CitH3) was used to label NETs, and Cyanine 5 (Cy5) was used to label liposomes during sample processing. In the PB-NEBP liposomes targeting group, more red fluorescent nanocomplexes were tightly bound around NETs, indicating that this targeting nanocomplex has a unique ability to actively target and activate neutrophils. However, almost no red fluorescent nanocomplexes were observed around the cells in the nontargeting group.

Protective effect on endothelial cells

[36,37] Increased ROS expression in local thrombi and vascular endothelial injury are the main pathological manifestations of DVT during pregnancy, and damage to ROS and the endothelium will lead to a series of signaling cascade reactions, such as inflammation and repair.[38] Platelets activate and adhere to the vascular endothelium and sites with high ROS expression,[39] recruiting inflammatory cells in the blood to the thrombus. Activated platelets and related factors secreted by inflammatory cells inhibit the proliferation and migration of vascular endothelial cells, promote cell apoptosis, slow endothelial recovery, and form a vicious cycle.[40] Therefore, the protective effect on the endothelium is particularly important. According to the experimental results in Figures 3B and 3C, the results from quantitative analysis demonstrated that H$_2$O$_2$-stimulated human umbilical vein endothelial cells (HUVECs) exhibited higher levels of intracellular ROS compared to normal cells. When H$_2$O$_2$-stimulated HUVECs were treated with NEBP liposomes, there was no significant change in intracellular ROS levels, indicating that NEBP liposomes were unable to remove ROS. On the other hand, PB NPs and PB-NEBP liposomes significantly reduced intracellular ROS levels. This further supports the notion that the ROS scavenging ability of PB-NEBP liposomes was attributed to the presence of PB NPs within it. After vascular endothelial injury, the recruitment, migration, and proliferation of endothelial cells at the injury site are crucial for the regulation of endothelial
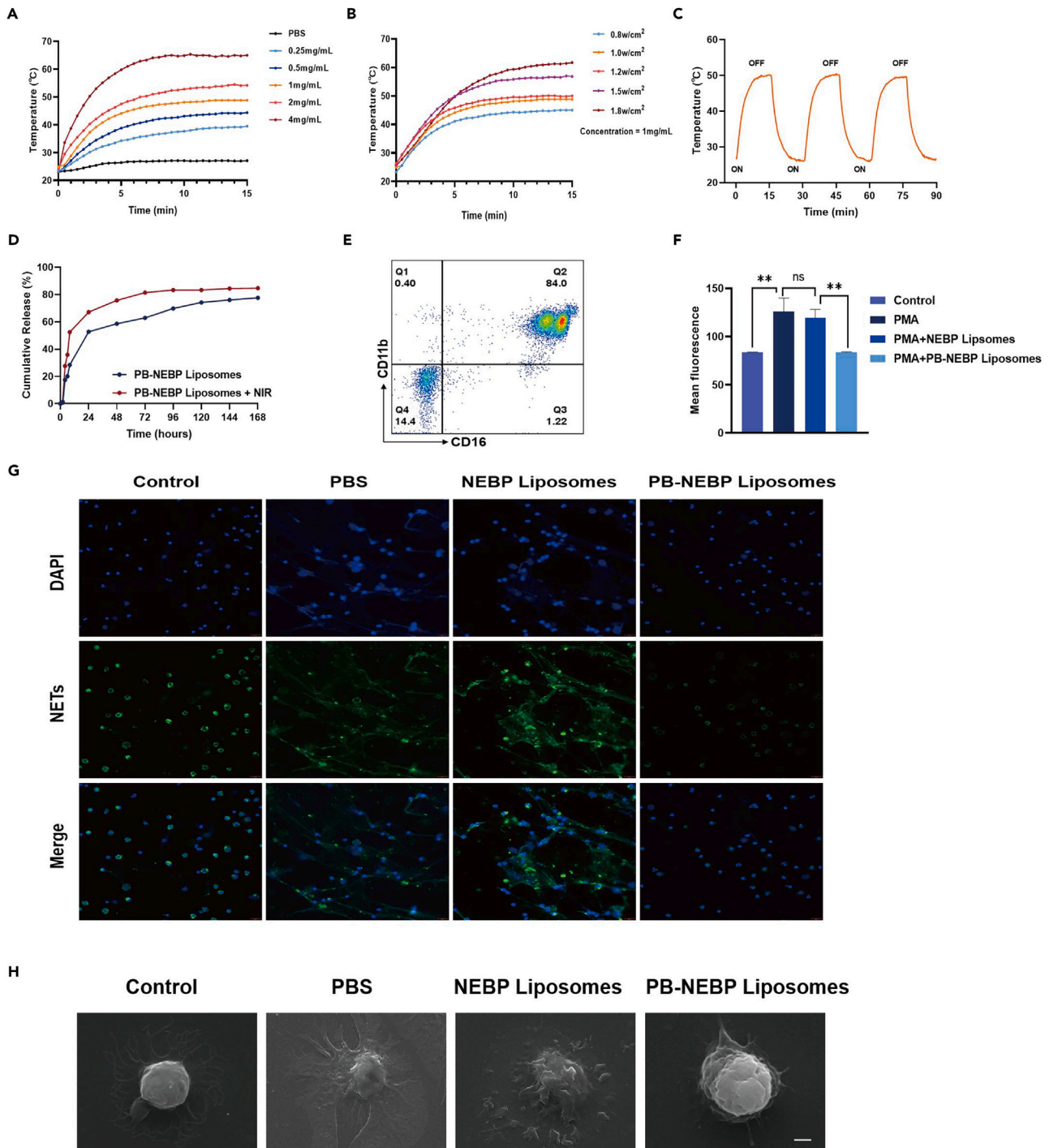
Figure 2. Photothermal performance and PB NPs release *in vitro*

(A) Temperature curves of PBS and PB-NEBP liposomes at various concentrations (0.25, 0.5, 1, 2, and 4 mg/mL) under irradiation at a power density of 1.2 W/cm^2 for 15 min.

(B) Temperature curves of PB-NEBP liposomes with a fixed concentration of 1 mg/mL at different NIR laser intensities (0.8, 1.0, 1.2, 1.5, and 1.8 W/cm^2) for 15 min.

(C) Temperature curves of PB-NEBP liposomes after three on/off cycles of photothermal heating (1 mg/mL, 1.2 W/cm^2).

(D) Cumulative release curve with or without treating with NIR.

(E) Flow cytometric assessments of human neutrophil purity.

(F) Statistical graph of average fluorescence intensity of NETs.

(G) Inhibiting effects on NETs of PBS and different liposomes. Data are reported as mean ± SD (*n* = 3 replicates); Scale bar, 20 μm.

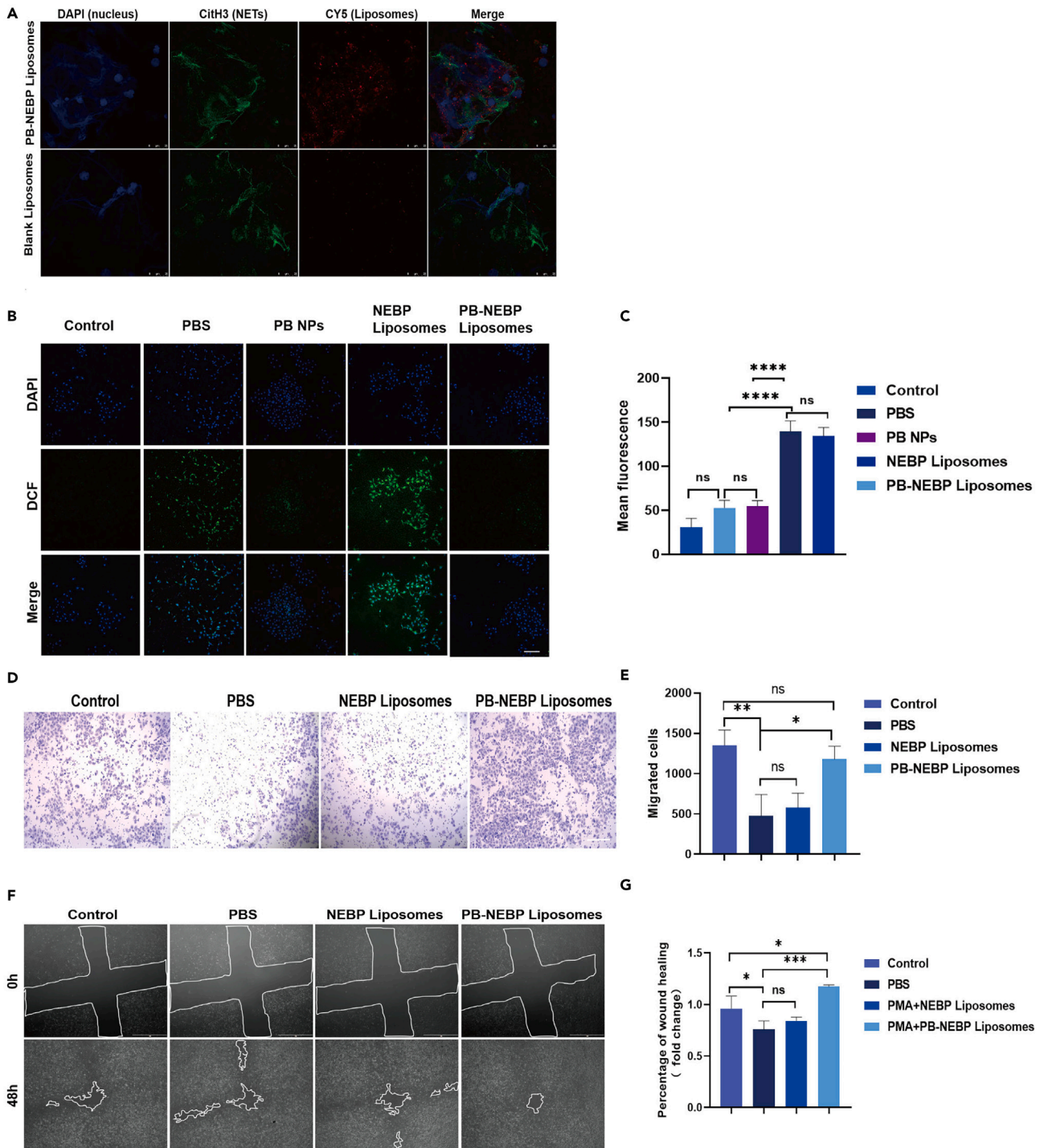(H) SEM of neutrophils in different experimental groups, Scale bar, 5 μm.

Figure 3. *In vitro* biological effects of PB-NEBP liposomes

(A) CLSM images of targeting ability of PMA-activated neutrophils *in vitro*. Red fluorescence shows Cy5-labeled liposomes; scale bar, 25 μm.

(B) ROS scavenging in HUVECs with different treatments.

(C) Quantitative analysis of the intracellular ROS levels in HUVECs. Data are reported as mean ± SD (*n* = 3 replicates); scale bar, 200 μm.

(D) Microscopic images and (E) quantitative analysis of migrated HUVECs after adding supernatant of different group and incubating for 48 h. Data are reported as mean ± SD (*n* = 3 replicates); scale bar, 50 μm.

(F) Microscopic images and (G) quantified analysis of wound healing based on the wound healing assay after separate incubation with PBS and supernatant of different group. Data are reported as mean ± SD (*n* = 3 replicates); Scale bar, 1 mm.
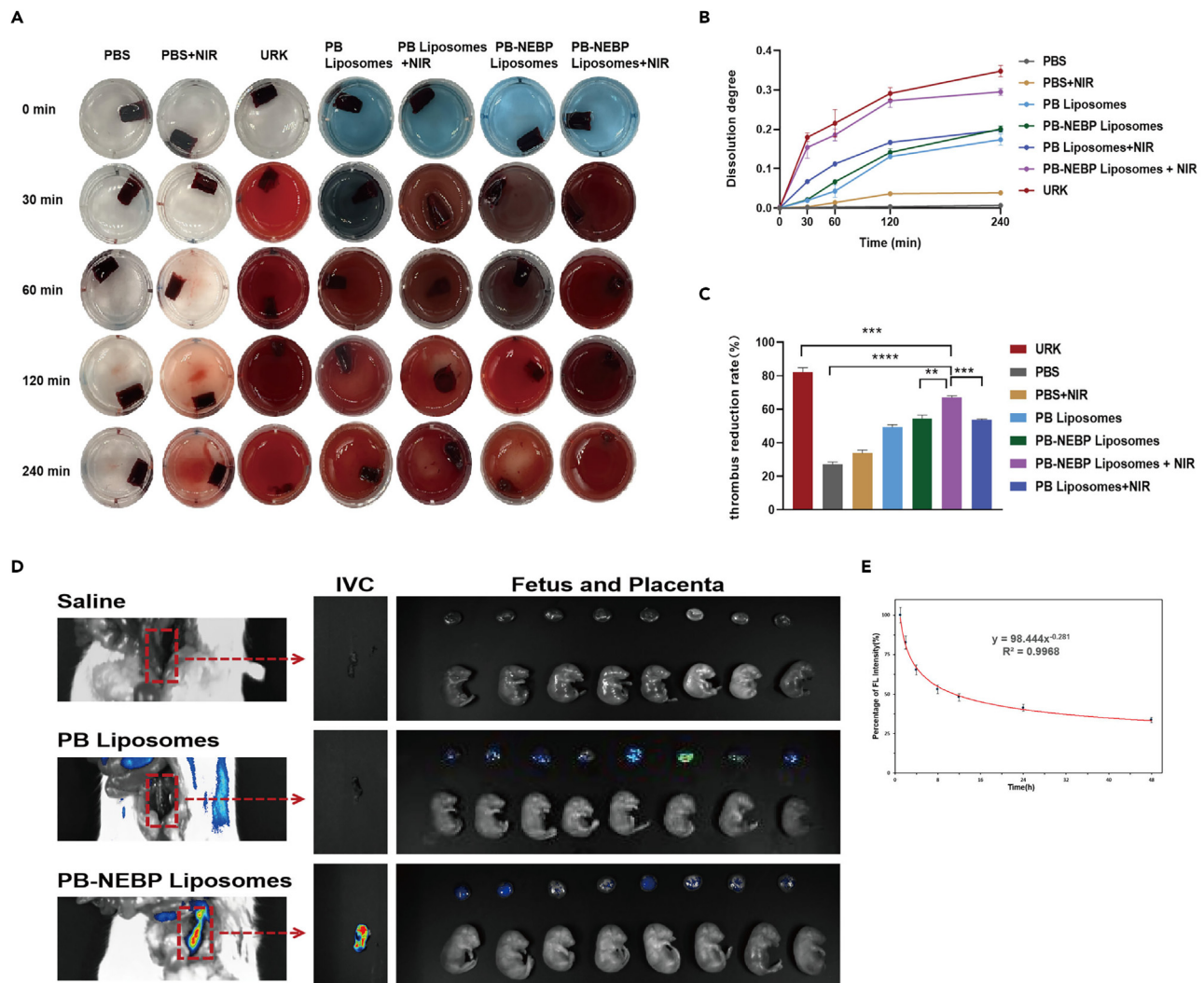
Figure 4. Thrombolysis assay and targeting ability of PB-NEBP liposomes *in vivo*

(A) Representative images of blood thrombus treated with different treatments at 5 selected time points, NIR laser irradiation (1.2 W/cm^2, 15 min).

(B) Final thrombus reduction rate of blood clots and (C) hemolysis rate after different treatments in each group. Data are reported as mean ± SD (n = 3 replicates).

(D) *In vivo* fluorescence images of the inferior vena cava thrombus in ICR mice from the saline group, nontargeted group (PB liposomes), and targeted group (PB-NEBP liposomes) after injection. *Ex vivo* fluorescence images of the inferior vena cava thrombus, fetus, and placenta (n = 3 replicates).

(E) Circulating metabolism of PB-NEBP liposomes in plasma (n = 3 replicates).

homeostasis.[41,42] Supernatants of each group were harvested and added into HUVECs. The aforementioned experiments simulated the microenvironment of the thrombus site. Activated neutrophils caused endothelial cell damage through NET-mediated increase of ROS levels. The results of the Transwell experiment (Figures 3D and 3E) showed that compared with the blank control group, the PB-NEBP liposomes group significantly promoted the migration of vascular endothelial cells after intervention, and the cell scratch experiment (Figures 3F and 3G) also proved that PB-NEBP liposomes can more significantly promote endothelial cell migration to promote wound healing. Through Transwell and cell scratch experiments, PB-NEBP liposomes significantly promoted the proliferation and migration of HUVECs and accelerated the repair of damaged endothelium.

Thrombolysis assay *in vitro*

After different treatments, thrombolysis was observed in all groups (Figure 4A). In no PTT groups, the dissolution degree (Figure 4B) and thrombus reduction rate (Figure 4C) in targeted group (PB-NEBP liposomes) was slightly higher than that in non-targeted group (PB liposomes). Compared with no PTT group, the thrombus in PB-NEBP liposomes group was significantly reduced in the PTT group. In general, pictures and quantitative analysis (Figures 4A–4C) show that PB-NEBP liposomes + NIR turns out to be more reliable and effective in thrombolysis assay, which provide a basis for further *in vivo* research.

Targeting and therapeutic effects of PB-NEBP liposomes *in vivo*

To verify the targeting ability of PB-NEBP liposomes, saline, Cy5-labeled PB liposomes, and Cy5-labeled PB-NEBP liposomes were administered via tail vein injection to pregnant mice. In the model group, inferior vena cava thrombosis was induced using 10% FeCl$_3$.[43] *In vivo* imaging revealed considerable accumulation of Cy5-labeled PB-NEBP liposomes at the thrombus site of the inferior vena cava (Figure 4D). *In vivo* fluorescence images indicated the thrombosis-targeting ability of PB-NEBP liposomes. In this experiment, the presence of fluorescence signals on the maternal side of the placenta is crucial, but no signals were found in the placental umbilical cord and fetus body. Previous studies have also investigated the distribution of different nanoparticle platforms in the placenta and fetus. Our own research supports these findings, as we observed no placental transportation or luciferase expression in the fetus when using PB-NEBP liposomes measuring 146 ± 3 nm. Aside from the various tight junctions that regulate placental transportation, it has been theorized that this size-dependent effect is attributable to the presence of transtrophoblastic channels.[44–48] It is theorized that nanoparticles with a diameter larger than 20 nm may not be able to utilize these channels to reach the fetal circulation.[44,49] This suggests that although nanomedicine can reach the maternal side of the placenta through blood circulation, it cannot penetrate the fetal-placental barrier and reach the fetal mice.

Inspired by the excellent performance of PB-NEBP liposomes *in vitro*, we further detected the thrombolysis effects on the inferior vena cava of pregnant mice. Pregnant mice randomly divided into 4 groups. The temperature changes of the inferior vena cava thrombosis site during the irradiation process were shown in Figure 5A. Figure 5B showed the infrared thermal image of thrombosis site. After irradiated for 15 min, the temperature of PB-NEBP liposomes group reached to 44.9°C and the temperature of PB liposomes group reached to 40.7°C. Compared with PB-NEBP liposomes group *in vivo*, the temperature was lower than that *in vitro* due to the blood flow. The temperature changes in control group and normal group are basically the same, both lower than that in the PB-NEBP liposomes and PB liposomes group.

We used FeCl$_3$ to establish an inferior vena cava thrombosis model in pregnant mice on day G14.5. At 1 h after model establishment, we injected saline, NEBP liposomes, PB liposomes, and PB-NEBP liposomes into the tail vein. Thrombus site is treated with NIR laser irradiation for 15 min at 1 h after injection. Based on the *in vivo* half-life detection results (Figure 4E) of PB-NEBP liposomes, repeat the aforementioned treatment after 12 h. The pregnant mice were sacrificed after anesthesia on day G17.5; the main organs, inferior vena cava thrombosis segment, fetuses, and placentas were collected. ELISA results proved that the PB-NEBP liposomes can significantly reduce the expression of the inflammatory factors IL-1β, IL-6, and TNF-α (Figures 5C–5E) in vascular grinding fluid to protect the vascular endothelium under inflammatory conditions. H&E staining of the venous thrombus site showed that both PB liposomes and PB-NEBP liposomes had broken thrombi, and the PB-NEBP liposomes cohort had the best destruction effect due to its ability to actively target thrombi combined with the PTT effect (Figure 5F). Based on the weight statistics of fetuses and placentae (Figures 5G and 5H), it was observed that the weight of placenta and fetus in the saline cohort and PB-NEBP liposomes cohort was significantly lower than that of the control cohorts. We speculate that this might relate to impaired placental function and decreased placental perfusion caused by the thrombus of the inferior vena cava. The weight of placental and fetuses in PB-NEBP liposomes cohort was higher than that in control cohort, suggesting that the PB-NEBP liposomes treatment also had a positive effect on fetal growth. This finding suggests that effective thrombolytic treatment can potentially reduce inflammatory factors in the blood, increase blood supply to the placenta, and facilitate fetal development. In summary, due to the antioxidant activity of PB-NEBP liposomes combined with the PTT effect, it can achieve an integrated antithrombotic treatment of thrombolysis, ROS scavenging, and inflammatory factors. Moreover, it can be made to effectively promote fetal growth and development.

Safety studies

Finally, we tested the safety of PB-NEBP liposomes. *In vitro* evaluation of HUVECs showed that PB-NEBP liposomes exhibited low cytotoxicity even at the maximum dose tested at approximately 8 mg/mL (Figure 6A). In addition, *in vitro* experiments showed that no obvious hemolysis was observed when PB-NEBP liposomes at different concentrations were cocultured with red blood cells (Figure 6B). To exclude the influence of the lower limb venous thrombosis model on pregnant mice, we injected physiological saline and PB-NEBP liposome into the tail vein of mice in the physiological pregnancy group, collected peripheral blood of pregnant mice on day 17.5, killed the pregnant mice after anesthesia, and recorded fetus number of mice, body weight, and H&E staining of main organs of pregnant mice. As shown in Figures 6E–6H, the prothrombin time, thrombin time, activated partial thromboplastin time, and fibrinogen content were detected to evaluate the changes in coagulation function of pregnant mice. The results showed that all indicators were within the normal range of the coagulation function of pregnant mice. In addition, the liver and kidney functions of pregnant mice were analyzed, and the results showed that alanine transaminase, aspartate transaminase, blood urea nitrogen, and creatinine were all normal, indicating that PB-NEBP liposomes had no significant effect on liver and kidney function in mice (Figures 6I–6L). H&E staining results showed that there were no histopathological abnormalities, such as inflammation or tissue damage, in the tissue sections of the treatment group (Figure 6M). In the study of PB-NEBP liposomes on the offspring of fetus mice, we found that the weight of placenta and fetal mice in the treatment group was not significantly different from that in the physiological group (Figures 6C and 6D). In addition, by double-staining the bones of fetus mice with alizarin red and Alcian blue (Figure 6N), there was no significant difference in bone content and cartilage content in the treatment groups. These preliminary studies suggested that PB-NEBP liposomes are safe for pregnant mice and do not cause fetal growth restriction or fetal bone development disorders.
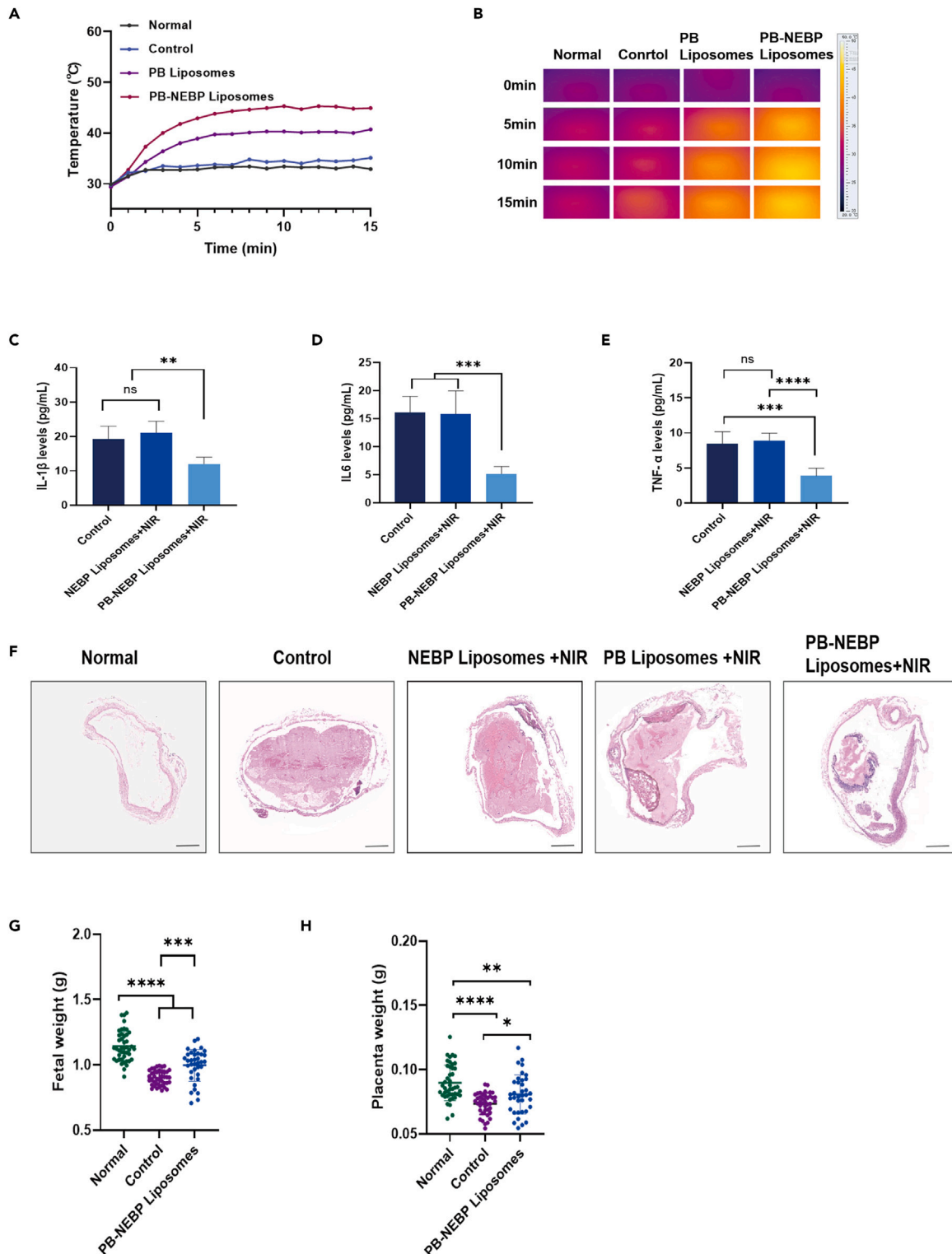
Figure 5. Therapeutic effects of PB-NEBP liposomes *in vivo*

(A) Temperature variation curves *in vivo* with an applied NIR laser (1.2 W/cm^2, 15 min).

(B) Corresponding thermal images of the thrombus site after NIR laser irradiation.

(C–E) Expression of the inflammatory factors IL-1β, IL-6, and TNF-α in inferior vena cava thrombosis via ELISA (*n* = 4 replicates).

(F) H&E staining of the inferior vena cava after various treatment; scale bar, 500 μm.

(G and H) The weight of fetus and placenta from 4 pregnant mice in normal cohort, control cohort, and PB-NEBP liposomes cohort.
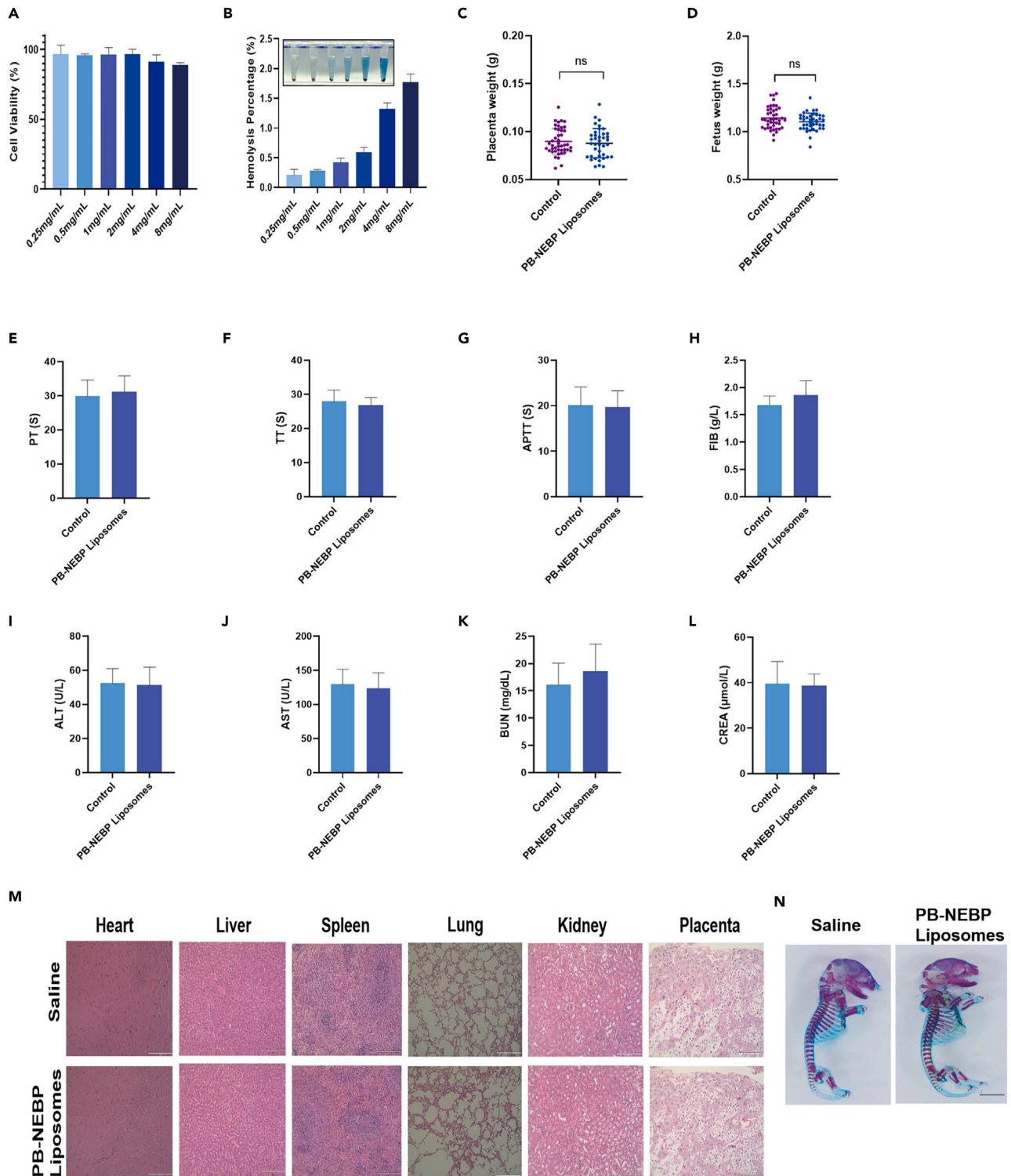
Figure 6. Evaluation of toxicity of PB-NEBP liposomes

(A) HUVECs viability at different PB-NEBP liposomes concentrations, detected by the CCK-8 method (n = 3 replicates).

(B) The hemolysis rate of the PB-NEBP liposomes in different concentrations (n = 3 replicates).

(C and D) The weight of placenta and fetus in normal cohort and PB-NEBP liposomes cohort (n = 5 replicates).

Figure 6. Continued

(E–H) Comparison of coagulation function including the prothrombin time (PT), activated partial thromboplastin time (APTT), thrombin time (TT), and fibrinogen content (fibrinogen, FIB) between control group and PB-NEBP liposomes group (n = 5 replicates).

(I–L) Comparison of the liver and kidney functions of pregnant mice including alanine transaminase (ALT), aspartate transaminase (AST), blood urea nitrogen (BUN), and creatinine (CREA) between control group and PB-NEBP liposomes group (n = 5 replicates).

(M) Histopathological images of the organs of ICR mice after 48 h of intravenous exposure to PB-NEBP liposomes, (n = 5 replicates); scale bar, 200 μm.

(N) Whole-mount skeletal staining of fetuses via Alcian blue and alizarin red S in different groups at G17.5; scale bar, 5 mm.

DISCUSSION

The increased hypercoagulable state brought on by physiological changes during pregnancy is likely an evolutionary protective mechanism against hemorrhaging during childbirth, but it also marks pregnancy as a strong risk factor for DVT. The latest research shows that NETs are involved in the formation of DVT during pregnancy, including platelet adhesion, production of ROS, activation of inflammatory factors, increased expression of anticoagulant factors, and destruction of endothelial cells. Therefore, we designed a multifunctional nanoplatform targeting NE in NETs loaded with PB NPs that can scavenge ROS, inhibit inflammatory factors, and have photothermal conversion capabilities and applied it to the treatment of DVT in pregnancy for the first time. Preliminary experiments have confirmed that PB-NEBP liposomes have reliable targeting of NETs *in vivo* and *in vitro* and good photothermal conversion efficiency and can be treated in a highly localized manner without the need for systemic anticoagulant drug treatment, minimizing the risk of long-term drug use side effect. In accordance with these findings, the administration of PB-NEBP liposomes treatment showed pronounced effects in terms of reversing the reduction in weight of both fetuses and placentas and rescued intrauterine growth restriction caused by maternal thrombosis. In this experiment, the higher-than-therapeutic dose of PB-NEBP liposomes did not penetrate the placental barrier and would not affect the health and pregnancy out-comes of the mother mice or the growth and development of the fetal mice. This provides positive significance for the clinical translation of this multifunctional nanoplatform.

It is worth noting that NETs are not only involved in the formation of thrombi but are also involved in diseases whose pathogenesis is not yet clear, such as gestational diabetes, premature birth, and preeclampsia. Therefore, a multifunctional loading platform targeting NETs may become a potential idea for the treatment of pregnancy-related diseases.

Limitations of the study

This study introduces a multifunctional nanoplatform targeting NET for the treatment of DVT in pregnancy. Further investigation is warranted to explore the potential causes of fetal growth restriction induced by DVT during pregnancy in the animal thrombosis model. In addition, literature reports have highlighted the potential of nanomaterial-based drugs in effectively treating thrombosis. Despite promising results, there is a lack of experimental studies utilizing these nanomedicines for pregnancy-related thrombotic diseases. This gap may be attributed to concerns regarding drug toxicity and their potential impact on fetal growth and development. Further research is needed to explore the application of nanomedicines in treating pregnancy-related thrombotic diseases, with the aim of enhancing treatment efficacy and reducing adverse pregnancy outcomes.

STAR★METHODS

Detailed methods are provided in the online version of this paper and include the following:

- KEY RESOURCES TABLE
- RESOURCE AVAILABILITY
  - Lead contact
  - Materials availability
  - Data and code availability
- EXPERIMENTAL MODEL AND STUDY PARTICIPANT DETAILS
  - Peripheral blood from volunteer
  - Animal
- METHOD DETAILS
  - Preparation of PB NPs
  - Preparation and characterization of the nanoparticles
  - Determination of reactive oxygen species-scavenging capability of PB-NEBP liposomes
  - Photothermal performance and PB NPs release *in vitro*
  - Inhibiting effects on NETs
  - Effect of targeting activated neutrophils *in vitro*
  - Protective effect on endothelial cells
  - Thrombolysis assay *in vitro*
  - Targeting capability and efficacies of PB-NEBP liposomes in pregnant mice with DVT
  - Evaluation of toxicity of PB-NEBP liposomes
- QUANTIFICATION AND STATISTICAL ANALYSIS

AUTHOR CONTRIBUTIONS

Y.Z.: conceptualization, methodology, data curation, and writing – original draft preparation; L.X.: software and investigation; P.J.: formal analysis and validation; N.L.: software; X.C.: writing – review and editing and project administration; A.Y.: project administration; H.Q.: supervision and funding acquisition.

DECLARATION OF INTERESTS

The authors declare no competing interests.

REFERENCES

1. Scheres, L.J.J., Lijfering, W.M., Groenewegen, N.F.M., Koole, S., de Groot, C.J.M., Middeldorp, S., and Cannegieter, S.C. (2020). Hypertensive Complications of Pregnancy and Risk of Venous Thromboembolism. Hypertension 75, 781–787.

2. Heit, J.A., Kobbervig, C.E., James, A.H., Petterson, T.M., Bailey, K.R., and Melton, L.J., 3rd (2005). Trends in the incidence of venous thromboembolism during pregnancy or postpartum: a 30-year population-based study. Ann. Intern. Med. 143, 697–706.

3. Abe, K., Kuklina, E.V., Hooper, W.C., and Callaghan, W.M. (2019). Venous thromboembolism as a cause of severe maternal morbidity and mortality in the United States. Semin. Perinatol. 43, 200–204.

4. James, A.H., Jamison, M.G., Brancazio, L.R., and Myers, E.R. (2006). Venous thromboembolism during pregnancy and the postpartum period: incidence, risk factors, and mortality. Am. J. Obstet. Gynecol. 194, 1311–1315.

5. Kruger, P.C., Eikelboom, J.W., Douketis, J.D., and Hankey, G.J. (2019). Deep vein thrombosis: update on diagnosis and management. Med. J. Aust. 210, 516–524.

6. Tran, H.A., Gibbs, H., Merriman, E., Curnow, J.L., Young, L., Bennett, A., Tan, C.W., Chunilal, S.D., Ward, C.M., Baker, R., and Nandurkar, H. (2019). New guidelines from the Thrombosis and Haemostasis Society of Australia and New Zealand for the diagnosis and management of venous thromboembolism. Med. J. Aust. 210, 227–235.

7. Khan, F., Vaillancourt, C., and Bourjeily, G. (2017). Diagnosis and management of deep vein thrombosis in pregnancy. BMJ 357, j2344.

8. Hastie, R., Tong, S., Wikström, A.K., Sandström, A., Hesselman, S., and Bergman, L. (2021). Aspirin use during pregnancy and the risk of bleeding complications: a Swedish population-based cohort study. Am. J. Obstet. Gynecol. 224, 95.e1–95.e12.

9. Zierler, S., and Rothman, K.J. (1985). Congenital heart disease in relation to maternal use of Bendectin and other drugs in early pregnancy. N. Engl. J. Med. 313, 347–352.

10. Monagle, P., Cuello, C.A., Augustine, C., Bonduel, M., Brandão, L.R., Capman, T., Chan, A.K.C., Hanson, S., Male, C., Meerpohl, J., et al. (2018). American Society of Hematology 2018 Guidelines for management of venous thromboembolism: treatment of pediatric venous thromboembolism. Blood Adv. 2, 3292–3316.

11. Gándara, E., Carrier, M., and Rodger, M.A. (2014). Management of pregnancy associated venous-thromboembolism: a survey of practices. Thromb. J. 12, 12.

12. Brinkmann, V., Reichard, U., Goosmann, C., Fauler, B., Uhlemann, Y., Weiss, D.S., Weinrauch, Y., and Zychlinsky, A. (2004). Neutrophil extracellular traps kill bacteria. Science 303, 1532–1535.

13. Thålin, C., Hisada, Y., Lundström, S., Mackman, N., and Wallén, H. (2019). Neutrophil Extracellular Traps: Villains and Targets in Arterial, Venous, and Cancer-Associated Thrombosis. Arterioscler. Thromb. Vasc. Biol. 39, 1724–1738.

14. Darboussett, R., Thomas, G.M., Mezouar, S., Frère, C., Bonier, R., Mackman, N., Renné, T., Dignat-George, F., Dubois, C., and Panicot-Dubois, L. (2012). Tissue factor-positive neutrophils bind to injured endothelial wall and initiate thrombus formation. Blood 120, 2133–2143.

15. Savchenko, A.S., Martinod, K., Seidman, M.A., Wong, S.L., Borissoff, J.I., Piazza, G., Libby, P., Goldhaber, S.Z., Mitchell, R.N., and Wagner, D.D. (2014). Neutrophil extracellular traps form predominantly during the organizing stage of human venous thromboembolism development. J. Thromb. Haemostasis 12, 860–870.

16. Varjú, I., and Kolev, K. (2019). Networks that stop the flow: A fresh look at fibrin and neutrophil extracellular traps. Thromb. Res. 182, 1–11.

17. Gollomp, K., Kim, M., Johnston, I., Hayes, V., Welsh, J., Arepally, G.M., Kahn, M., Lambert, M.P., Cuker, A., Cines, D.B., et al. (2018). Neutrophil accumulation and NET release contribute to thrombosis in HIT. JCI Insight 3, e99445.

18. Urban, C.F., Ermert, D., Schmid, M., Abu-Abed, U., Goosmann, C., Nacken, W., Brinkmann, V., Jungblut, P.R., and Zychlinsky, A. (2009). Neutrophil extracellular traps contain calprotectin, a cytosolic protein complex involved in host defense against Candida albicans. PLoS Pathog. 5, e1000639.

19. Dhayalan, M., Wang, W., Riyaz, S.U.M., Dinesh, R.A., Shanmugam, J., Irudayaraj, S.S., Stalin, A., Giri, J., Mallik, S., and Hu, R. (2024). Advances in functional lipid nanoparticles: from drug delivery platforms to clinical applications. 3 Biotech 14, 57.

20. Allen, T.M., and Cullis, P.R. (2013). Liposomal drug delivery systems: from concept to clinical applications. Adv. Drug Deliv. Rev. 65, 36–48.

21. Stoiber, W., Obermayer, A., Steinbacher, P., and Krautgartner, W.D. (2015). The Role of Reactive Oxygen Species (ROS) in the Formation of Extracellular Traps (ETs) in Humans. Biomolecules 5, 702–723.

22. Kim, K., Li, J., Tseng, A., Andrews, R.K., and Cho, J. (2015). NOX2 is critical for heterotypic neutrophil-platelet interactions during vascular inflammation. Blood 126, 1952–1964.

23. Gao, Y., Yu, G., Xing, K., Gorin, D., Kotelevtsev, Y., Tong, W., and Mao, Z. (2020). Finely tuned Prussian blue-based nanoparticles and their application in disease treatment. J. Mater. Chem. B 8, 7121–7134.

24. Sahu, A., Lee, J.H., Lee, H.G., Jeong, Y.Y., and Tae, G. (2016). Prussian blue/serum albumin/indocyanine green as a multifunctional nanotheranostic agent for bimodal imaging

guided laser mediated combinatorial phototherapy. J. Contr. Release 236, 90–99.

25. Gao, X., Wang, Q., Cheng, C., Lin, S., Lin, T., Liu, C., and Han, X. (2020). The Application of Prussian Blue Nanoparticles in Tumor Diagnosis and Treatment. Sensors 20, 6905.

26. Cao, Z., Zhang, X., Wei, Z., Song, C., Zou, H., Ran, J., Zhang, H., Xie, D., Han, S., Wang, Y., et al. (2022). Thrombus-targeted nano-agents for NIR-II diagnostic fluorescence imaging-guided flap thromboembolism multi-model therapy. J. Nanobiotechnol. 20, 447.

27. Liang, X., Deng, Z., Jing, L., Li, X., Dai, Z., Li, C., and Huang, M. (2013). Prussian blue nanoparticles operate as a contrast agent for enhanced photoacoustic imaging. Chem. Commun. 49, 11029–11031.

28. Garcia-Uribe, A., Erpelding, T.N., Krumholz, A., Ke, H., Maslov, K., Appleton, C., Margenthaler, J.A., and Wang, L.V. (2015). Dual-Modality Photoacoustic and Ultrasound Imaging System for Noninvasive Sentinel Lymph Node Detection in Patients with Breast Cancer. Sci. Rep. 5, 15748.

29. Chen, Z., Wang, G., Xie, X., Liu, H., Liao, J., Shi, H., Chen, M., Lai, S., Wang, Z., and Wu, X. (2022). Ginsenoside Rg5 allosterically interacts with P2RY(12) and ameliorates deep venous thrombosis by counteracting neutrophil NETosis and inflammatory response. Front. Immunol. 13, 918476.

30. Radermecker, C., Detrembleur, N., Guiot, J., Cavalier, E., Henket, M., d'Emal, C., Vanwinge, C., Cataldo, D., Oury, C., Delvenne, P., and Marichal, T. (2020). Neutrophil extracellular traps infiltrate the lung airway, interstitial, and vascular compartments in severe COVID-19. J. Exp. Med. 217, e20201012.

31. Bonilla, M.C., Quiros, O.N., Wendt, M., Hennig-Pauka, I., Mörgelin, M., von Köckritz-Blickwede, M., and de Buhr, N. (2022). New Insights into Neutrophil Extracellular Trap (NETs) Formation from Porcine Neutrophils in Response to Bacterial Infections. Int. J. Mol. Sci. 23, 8953.

32. Li, M., Lin, C., Leso, A., and Nefedova, Y. (2020). Quantification of Citrullinated Histone H3 Bound DNA for Detection of Neutrophil Extracellular Traps. Cancers 12, 3424.

33. Jorch, S.K., and Kubes, P. (2017). An emerging role for neutrophil extracellular traps in noninfectious disease. Nat. Med. 23, 279–287.

34. Keszei, M., Record, J., Kritikou, J.S., Wurzer, H., Geyer, C., Thiemann, M., Drescher, P., Brauner, H., Köcher, L., James, J., et al. (2021). Constitutive activation of WASp in X-linked neutropenia renders neutrophils hyperactive. J. Clin. Invest. 131, e156513.

35. Cruz, M.A., Bohinc, D., Andraska, E.A., Alvikas, J., Raghunathan, S., Masters, N.A., van Kleef, N.D., Bane, K.L., Hart, K., Medrow, K., et al. (2022). Nanomedicine platform for targeting activated neutrophils and neutrophil-platelet complexes using an α(1)-antitrypsin-derived peptide motif. Nat. Nanotechnol. 17, 1004–1014.

36. Nishimura, S., Manabe, I., Nagasaki, M., Kakuta, S., Iwakura, Y., Takayama, N., Ooehara, J., Otsu, M., Kamiya, A., Petrich, B.G., et al. (2012). In vivo imaging visualizes discoid platelet aggregations without endothelium disruption and implicates contribution of inflammatory cytokine and integrin signaling. Blood 119, e45–e56.

37. Machlus, K.R., Lin, F.C., and Wolberg, A.S. (2011). Procoagulant activity induced by vascular injury determines contribution of elevated factor VIII to thrombosis and thrombus stability in mice. Blood 118, 3960–3968.

38. Jiang, J., Zhan, X., Qu, H., Liang, T., Li, H., Chen, L., Huang, S., Sun, X., Jiang, W., Chen, J., et al. (2022). Upregulated of ANXA3, SORL1, and Neutrophils May Be Key Factors in the Progressionof Ankylosing Spondylitis. Front. Immunol. 13, 861459.

39. Sivaraman, B., and Latour, R.A. (2011). Delineating the roles of the GPIIb/IIIa and GP-Ib-IX-V platelet receptors in mediating platelet adhesion to adsorbed fibrinogen and albumin. Biomaterials 32, 5365–5370.

40. Rudolph, J.M., Guttek, K., Weitz, G., Meinke, C.A., Kliche, S., Reinhold, D., Schraven, B., and Reinhold, A. (2019). Characterization of Mice with a Platelet-Specific Deletion of the Adapter Molecule ADAP. Mol. Cell Biol. 39, e00365-18.

41. Liu, C., Yao, M.D., Li, C.P., Shan, K., Yang, H., Wang, J.J., Liu, B., Li, X.M., Yao, J., Jiang, Q., and Yan, B. (2017). Silencing Of Circular RNA-ZNF609 Ameliorates Vascular Endothelial Dysfunction. Theranostics 7, 2863–2877.

42. Birdsey, G.M., Dryden, N.H., Amsellem, V., Gebhardt, F., Sahnan, K., Haskard, D.O., Dejana, E., Mason, J.C., and Randi, A.M. (2008). Transcription factor Erg regulates angiogenesis and endothelial apoptosis through VE-cadherin. Blood 111, 3498–3506.

43. Zhang, S., Liu, Y., Wang, X., Yang, L., Li, H., Wang, Y., Liu, M., Zhao, X., Xie, Y., Yang, Y., et al. (2020). SARS-CoV-2 binds platelet ACE2 to enhance thrombosis in COVID-19. J. Hematol. Oncol. 13, 120.

44. Semmler-Behnke, M., Lipka, J., Wenk, A., Hirn, S., Schäffler, M., Tian, F., Schmid, G., Oberdörster, G., and Kreyling, W.G. (2014). Size dependent translocation and fetal accumulation of gold nanoparticles from maternal blood in the rat. Part. Fibre Toxicol. 11, 33.

45. Irvin-Choy, N.S., Nelson, K.M., Dang, M.N., Gleghorn, J.P., and Day, E.S. (2021). Gold nanoparticle biodistribution in pregnant mice following intravenous administration varies with gestational age. Nanomedicine 36, 102412.

46. Paul, J.W., Hua, S., Ilicic, M., Tolosa, J.M., Butler, T., Robertson, S., and Smith, R. (2017). Drug delivery to the human and mouse uterus using immunoliposomes targeted to the oxytocin receptor. Am. J. Obstet. Gynecol. 216, 283.e1–283.e14.

47. Alfaifi, A.A., Heyder, R.S., Bielski, E.R., Almuqbil, R.M., Kavdia, M., Gerk, P.M., and da Rocha, S.R.P. (2020). Megalin-targeting liposomes for placental drug delivery. J. Contr. Release 324, 366–378.

48. Ho, D., Leong, J.W., Crew, R.C., Norret, M., House, M.J., Mark, P.J., Waddell, B.J., Iyer, K.S., and Keelan, J.A. (2017). Maternal-placental-fetal biodistribution of multimodal polymeric nanoparticles in a pregnant rat model in mid and late gestation. Sci. Rep. 7, 2866.

49. Kertschanska, S., Stulcová, B., Kaufmann, P., and Stulc, J. (2000). Distensible transtrophoblastic channels in the rat placenta. Placenta 21, 670–677.

STAR★METHODS

KEY RESOURCES TABLE

REAGENT or RESOURCE	SOURCE	IDENTIFIER
Antibodies		
Anti-Histone H3	Abcam	Cat# ab281584; RRID:AB_11214865
Fluorescein (FITC)–conjugated Affinipure Goat Anti-Rabbit IgG (H+L)	Proteintech	Cat# SA00003-2; RRID:AB_10124381
Biological samples		
Peripheral blood of healthy donors	The First Affiliated Hospital of Chongqing Medical University, Chongqing, China	N/A
Chemicals, peptides, and recombinant proteins		
Neutrophil elastase binding peptide CGEAIPMSIPPEVK (NEBP)	Xi'an Ruixi Biological Technology Ltd.	N/A
Iron(III) chloride ($FeCl_3$)	Macklin Biochemical	Cat# I811935
Potassium ferrocyanide trihydrate solution ($K_4[Fe(CN)_6]$)	Macklin Biochemical	Cat# P787532
Phorbol 12-myristate 13-acetate (PMA)	Abcam	Cat# ab120297
Histopaque®-1077	Sigma-Aldrich	Cat# 10771
Histopaque®-1119	Sigma-Aldrich	Cat# 11191
Cyanine5 (Cy5) NHS ester	Xi'an Ruixi Biological Technology Ltd.	Cat# R-FR-004
DSPE-NEPB-PEG2000	Hefei Scierbio Tech Ltd	N/A
Cholesterol	Xi'an Ruixi Biological Technology Ltd.	Cat# R-H-100001
1,2-distearoyl-sn-glycero-3-phosphoethanolamine-N[methoxy (polyethylene glycol)-2000]	Xi'an Ruixi Biological Technology Ltd.	Cat# LP-R4-039
Distearyl phosphatidyl choline (DSPC)	Xi'an Ruixi Biological Technology Ltd.	Cat# R-Y-LZ-1018
Critical commercial assays		
Mouse IL-1 beta ELISA Kit	Servicebio Tech Ltd	Cat# GEM0002-96T
Mouse IL-6 ELISA Kit	Servicebio Tech Ltd	Cat# GEM0001-96T
Mouse TNF-alpha ELISA Kit	Servicebio Tech Ltd	Cat# GEM0004-96T
CCK-8 kit	Beyotime Biotechnology	Cat# C0038
Reactive Oxygen Species Assay Kit	Beyotime Biotechnology	Cat# S0033S
Experimental models: Cell lines		
Human umbilical vein endothelial cell (HUVECs)	ATCC	Cat# CRL-1730
Experimental models: Organisms/strains		
Female ICR mice	Shanghai SLAC Laboratory Animal Ltd.	N/A
Software and algorithms		
Prime 8.0	GraphPad Software	https://www.graphpad.com/
ImageJ	N/A	https://imagej.nih.gov/ij/

RESOURCE AVAILABILITY

Lead contact

Further information and requests for resources and reagents should be directed to and will be fulfilled by the lead contact, Xuehai Chen (cxh5256@gmail.com).

Materials availability

This study did not generate new unique reagents.

Data and code availability

- Data reported in this paper will be shared by the lead contact upon request.
- This paper does not report original code.
- Any additional information required to reanalyze the data reported in this paper is available from the lead contact upon request.

EXPERIMENTAL MODEL AND STUDY PARTICIPANT DETAILS

Peripheral blood from volunteer

9 healthy adult volunteers (3 males, 6 females) were recruited within an age range of 20-40, the average age was 29.3 years. All volunteers in this study were Han Chinese from Chongqing area. Peripheral blood from volunteer was collected under ethics approval from the First Affiliated Hospital of Chongqing Medical University (Ethical approval code: 2022-k222), and written informed consent for participation was obtained from all participants.

Animal

Female ICR mice (6–10 weeks old) were procured from Shanghai SLAC Laboratory Animal Ltd., getting housed with free access to standard food and water. All animal experiments were performed in accordance with Chinese rules for the use of animals in research. Ethical approval for this animal experiment was obtained from the Ethics Committee of the First Affiliated Hospital of Chongqing Medical University (Approval number: 2020-790).

METHOD DETAILS

Preparation of PB NPs

PB NPs were synthesized following well-established protocols, as outlined in the literature.[25] In a typical procedure, 0.5mmol citric acid was added into a 20 mL aqueous solution of $FeCl_3$ (1.0 mM) when continuous stirring at 60°C, subsequently, a 20 mL aqueous solution of $K_4[Fe(CN)_6]$ (1.0 mM), containing an equivalent amount of citric acid, was dropwise added to the above solution with stirring, while maintained at 60°C. Clear blue dispersion promptly formed during the amalgamation process, and the mixture was left to cool in room temperature, while stirring continued for an additional 30 minutes. For the collection of PB NPs, an equal volume of acetone was incorporated into the dispersion. The resultant mixture underwent centrifugation at 12500 rpm for 60 minutes, to precipitate the PB NPs. The collected precipitation was dialyzed for 24 h in distilled water. The morphology of the synthesized PB NPs was observed via TEM using a Hitachi H-7600 instrument, while the crystalline characteristics were elucidated through XRD analysis using a D8 ADVANCE instrument from Germany.

Preparation and characterization of the nanoparticles

PB-NEBP Liposomes were fabricated utilizing the thin-film hydration-sonication method. DSPE-NEPB-PEG2000 was synthesized by Hefei Scierbio Tech Ltd. Initially, Distearyl phosphatidyl choline (DSPC), cholesterol, and DSPE-NEPB-PEG2000 were meticulously dissolved in chloroform for 10 min. Subsequently, the mixture was removed to the round-bottom flask. After 1h 50°C rotary vacuum evaporation (RE-52A, Yarong, Shanghai, China), we obtained a uniform layer film. Kept within ice bath, 500 μL PB NPs solution (10 mg mL^{-1}) and 5 mL ddH$_2$O were added to the layer film, and the mixture underwent emulsification by ultrasonic probe at 125 W (VCX-130, Sonics & Materials, Inc., USA) for 6 min. Resultant products were collected by centrifuge (5804R; Eppendorf, Hamburg, Germany) at 8500 rpm for 5 min after each rinsed, The rinse and centrifuge were performed 3 times. Liposome extruder (polycarbonate membrane, pore size 200 nm) was utilized to eliminate free lipids and other reactants, followed by dialysis conducted via nanodialysis device (polycarbonate membrane, 50 nm pore size), to remove unencapsulated PB NPs. The preparation of PB Liposomes followed the same procedure, except for that DSPE-NEBP-PEG2000 was replaced by DSPE-mPEG2000. Morphological and structural characterization was conducted by transmission electron microscopy (TEM, Hitachi H-7600, Japan). Initially, liposomes (200 μL) were supplemented in ddH$_2$O to 10 mL. 1 drop was then extracted with precision using a syringe, and delicately deposited onto a 200-mesh copper grid. After drying, internal structure was visualized under TEM. Zeta potential and size distribution was determined by dynamic light scattering (DLS, Malvern Instruments, Malvern, UK). PB-NEBP Liposomes were incubated in PBS or PBS enriched with 10% FBS, the incubation temperature was 37°C. Samples were collected at various time (24 h, 72 h, 120 h, and 168 h) to assess changes in particle size. Size stability of PB-NEBP Liposomes was systematically monitored by DLS. PB loading ability was analyzed by UV-vis spectrophotometer (Puxi TU-1810, China) at 700 nm.

Determination of reactive oxygen species-scavenging capability of PB-NEBP liposomes

Electron paramagnetic resonance (EPR, Bruker A300-10/12, Germany) got used to determine hydroxyl radicals, hydrogen peroxide, peroxyl radicals and superoxide radicals scavenging abilities of PB-NEBP Liposomes.

Hydroxyl radicals scavenging

A FeSO$_4$ solution with 5 mg/mL concentration was configured. 200 μL of the solution was taken and mixed with 20 μL of 5,5-dimethyl-1-pyrro-line-N-oxide (DMPO) and 160 μL of PB-NEBP Liposomes solution (0.5mg/mL). Then, 20 μL of 30% hydrogen peroxide was added to the mixture, which was then mixed and allowed to react for 5 minutes. A sample was taken from this mixture and used as the experimental group data. In the control group, the PB-NEBP Liposomes was replaced with deionized water.

Hydrogen peroxide scavenging

In this study, H$_2$O$_2$ a mixture was prepared by combining 500 μL of 3-carbamoyl-2,5-dihydro-2,2,5,5-tetramethyl-1H-pyrrol-1-yloxyl (CTPO) solution with a concentration of 100 mM, 400 μL ofsolution with a concentration of 20 mM, and deionized water 100 μL. This mixture was then deoxygenated for a period of 30 minutes, serving as the control data. For the experimental group data, deionized water 100 μL was positioned with PB-NEBP Liposomes solution (0.5 mg/mL).

Peroxyl radicals scavenging

Dissolve C$_3$N$_4$ in the methanol solution, set the concentration to 1 mg/mL, and adjust the pH to about 5. Take 200 μL of this solution, add 200 μL of DMPO solution with a concentration of 100 mM and 100 μL of methanol, mix and illuminate for 10 minutes to collect data as the control. For test group, replace methanol 100 μL with 100 μL of samples PB-NEBP Liposomes solution (0.5 mg/mL).

Superoxide radicals scavenging

Xanthine solution with a precisely calibrated concentration of 10 mM, and xanthine oxidase solution maintained at 1 U/mL concentration, were prepared with PBS buffer as the solvent. Subsequently, 100 μL aliquots of the xanthine solution and the xanthine oxidase solution were combined, and to this mixture, 20 μL of DMPO and 180 μL PB-NEBP Liposomes solution (0.5 mg/mL) were supplemented. The mixture was incubated for 10 minutes and then sampled for testing.

Photothermal performance and PB NPs release *in vitro*

PB-NEBP Liposomes, spanning a spectrum of concentrations (0.25, 0.5, 1, 2, and 4 mg/mL), were systematically arranged in a 96-well plate. These liposomes were subsequently subjected to irradiation, with an 808 nm NIR laser (LR-ISP-808, China), operating at a power density of 1.2 W/cm^2 for 15 minutes. Following above procedure, PB-NEBP Liposomes, set at 1 mg/mL, underwent irradiation with varying NIR laser intensities (0.8, 1.0, 1.2, 1.5, and 1.8 W/cm^2) over a 15-minute interval. Thermal images were meticulously captured using an infrared thermal imaging system (Fluke Ti32, USA), from which a time-temperature curve was derived. To assess the resilience of the heat energy of PB-NEBP Liposomes, we subjected them to a high-temperature environment for 15 min, followed by natural cooling to room temperature, and repeated this procedure for three times. Additionally, we scrutinized the release dynamics of PB NPs from PB-NEBP Liposomes under NIR treatment (1.2 W/cm^2, 15 minutes), while untreated PB-NEBP Liposomes was set as control group. The supernatant got assiduously detected at 700 nm, at distinct time points, using a UV-vis spectrophotometer. Subsequently, the cumulative release percentage (%) of PB NPs was computed for various time points, and a comprehensive PB NPs release curve was meticulously delineated.

Inhibiting effects on NETs

Healthy volunteer blood was collected under ethics approval from the First Affiliated Hospital of Chongqing Medical University.[26] Neutrophils was meticulously isolated from the peripheral blood of healthy donors according to established methods. The purity of cell separation was evaluated by flow cytometry. 8×10^5 neutrophils were plated in a well of polylysine pretreated 12-well plate, PB-NEBP Liposomes, NEBP Liposomes and PBS groups treated with 100 nM PMA to stimulate NETs formation, and no PMA was added as control group. 200ul PBS, NEBP Liposomes and PB-NEBP Liposomes were added in the different experimental groups. 4 hours after incubation, NETs formation was evaluated by immunostaining (NETs were immunostained with anti-CitH3 antibody in green and DAPI for DNA labeling in blue). Fluorescence intensity was quantified using Image J software for further statistical analyses. The morphology of neutrophils was observed under Scanning electron microscopy (SEM).

Effect of targeting activated neutrophils *in vitro*

After co-culture with Cy5-labeled liposomes in PMA-activated neutrophils for 4h, The targeted localization of PB-NEBP Liposomes were observed by confocal laser scanning fluorescent microscopy (Nikon A1, Japan), Blank liposomes were used as nontargeting group.

Protective effect on endothelial cells

ROS was quantified by Reactive Oxygen Species Assay Kit. HUVECs were cultured for 24h. Subsequently, the cells were treated with PBS, fresh medium containing PB NPs, fresh medium containing NEBP Liposomes, and fresh medium containing PB-NEBP Liposomes. 200 μM H$_2$O$_2$ were added at the same time, while negative control cohort comprised untreated cells. 6 hours later cells were sent for PBS washing and a 10 μM DCFH-DA incubation for 30 min. After another PBS wash, cells were processed with 4% paraformaldehyde for 20 minutes, DAPI-staining (100 μL) for 15 minutes. The cells was visualized under scanning microscopy.

Neutrophils were stimulated with PMA (100nM) for 120 min, followed by the addition of 100 μL of medium, containing NEBP Liposomes and PB-NEBP Liposomes separately. The control group without PMA stimulation was included, with each group triplicated. After 6 hours, we conducted a centrifugation at room temperature for 10 min, the supernatant containing NETs was carefully collected and transferred to new labeled tubes. HUVECs were then planted within Transwell chamber upper compartment at 5×10^4 cells/well. 200 μL of supernatant from each group were added separately, fresh 1640 medium was supplemented to the bottom. Following 48h incubation, cells invading membrane was fixed, crystal violet-stained, and quantified using optical microscopy. In scratch wound healing assay, we cultured HUVECs in 6-well plates till reaching confluence. We created an incision utilizing micropipette tip (200 μL), supplementing 2 mL of supernatant from each group, and sent them for a 48h incubation, with fresh 1640 medium supplement as control. We randomly choose 3 visual fields and photograph them under microscope (EVOS™ FL Color Imaging System, Thermo Fisher Scientific), with 100× magnification. Migrating HUVECs was quantified with Image Pro Plus 6.0 software, the inhibition percentage was calculated. Assays were repeated trice across 3 independent experiments, images were captured under an optical microscope.

Thrombolysis assay *in vitro*

Fresh blood was collected from pregnant ICR mice and incubated at room temperature for 12 hours to prepare blood clots. The blood clots with equal weight were then divided into different groups (PBS group, PBS + NIR group, Urokinase group, PB Liposomes group, PB Liposomes + NIR group, PB-NEPB-Liposomes, and PB-NEPB-Liposomes + NIR group). Each group of blood clots was treated according to the respective grouping. Urokinase served as the positive control, while PBS functioned as the negative control. The near-infrared (NIR) power used for the treatment was 1.2 W/cm^2, with an irradiation time of 15 minutes. The concentration of the Liposomes solution added was 1 mg/mL. Post various treatments, the weight lost during the experiment was determined by calculating the disparity in blood clot weight, before and after immersion in the solutions of respective groups. To evaluate the efficacy of extracorporeal thrombolytic therapy, Release of hemoglobin were gauged by measuring the absorbance of the supernatant at 540 nm, detected via a microplate reader (Bio-Rad, Microplate Reader 550). Dissolution degree = $(OD_i - OD_0) / (t_i - t_0)$, where OD_i and OD_0 represent the absorbance at two consecutive time points t_i and t_0 respectively. This assessment was done to evaluate the effectiveness of extracorporeal thrombolytic therapy.

Targeting capability and efficacies of PB-NEBP liposomes in pregnant mice with DVT

A FeCl$_3$-induced inferior vena cava thrombosis pregnant ICR mice model

Female ICR mice (6–10 weeks old) were procured from Shanghai SLAC Laboratory Animal Ltd., getting housed with free access to standard food and water. Ethical approval for this animal experiment was obtained from the Ethics Committee of the First Affiliated Hospital of Chongqing Medical University (Approval number: 2020-790). To investigate the targeting precision and therapeutic efficacy of the nanoparticles, a pregnant ICR mouse model of FeCl$_3$-induced inferior vena cava thrombosis was established. The mice, anesthetized through continuous inhalation of isoflurane, were positioned in a supine posture after fur removal. The inferior vena cava of pregnant mice was exposed, a filter paper piece soaked in 10% FeCl$_3$ (1 mm × 2 mm) was applied to the inferior vena cava for 3 min to induce the formation of deep venous thrombosis. Subsequent to above procedure, any residual FeCl$_3$ was meticulously removed with saline. Doppler ultrasound was employed to confirm thrombus formation during the surgery, and a heating pad was utilized throughout the procedure to sustain the mouse's body temperature at 37°C.

Targeting capability of PB-NEBP liposomes in vivo

After the establishment of FeCl$_3$-induced DVT in pregnant mice, PB Liposomes, PB-NEBP Liposomes, saline were given at the same volume via the tail vein on Day G14.5. At 2 h after injection, expose the inferior vena cava of pregnant mice, observe the thrombus-vascular site in fluorescence intensity. At 12 h after injection mice were euthanized, we proceeded to dissect the uterus from pregnant mice to remove the placentas and corresponding fetuses. The inferior vena cava, along with major organs, got harvested. Following PBS rinsing, *ex vivo* imaging was completed via the OI600 MF Touch Multifunction Imager (BIO-OI Biotechnology Co., Ltd, China).

Therapeutic effects of PB-NEBP liposomes in pregnant mice with DVT

To evaluate temperature changes in the thrombus site, Pregnant mice were subsequently partitioned into 4 cohorts (n = 4): normal cohort; control cohort; PB Liposome cohort; PB-NEBP Liposomes cohort. Except normal cohort, DVT was induced in pregnant mice using FeCl$_3$ on day G14.5. Saline and above various liposomes (1 mg/mL, 0.2 mL) were intravenously injected, with an applied NIR laser energy intensity of 1.2W/cm^2 for 15 min, and a thermal imaging system that operates on infrared was utilized to observe and record alterations in temperature throughout the treatment process *in vivo*.

To assess PB-NEBP Liposomes therapeutic efficacy on thrombus *in vivo*, the mice were subsequently partitioned into 5 cohorts (n = 4): normal cohort, control cohort, NEBP Liposomes + NIR cohort, PB Liposome + NIR cohort, PB-NEBP Liposomes + NIR cohort. Except normal cohort, DVT was induced in pregnant mice using FeCl$_3$ on day G14.5. At 1 hour after model establishment, intravenous injections of saline and various liposomes (1 mg/mL, 0.2 mL) were administered to pregnant mice, accompanied by an NIR laser with 1.2W/cm^2 for 15 min. During treatment, infrared thermal imaging was employed to monitor *in vivo* temperature changes. Repeat the above treatment after 12 hours. Following three days of therapy, the pregnant mice were sacrificed after anesthesia, the main organs, inferior vena cava thrombosis segment, all fetuses and placentas were collected. The inferior vena cava was excised for HE staining and microscopic observation. The impact of IL-1β,

IL-6, and TNF-α levels in inferior vena cava thrombosis was detected via ELISA, referred from professional instructions (Mouse IL-1β, IL-6, TNF-α ELISA Kit, Servicebio, China). The weight of each fetus and placenta were weighed and recorded.

Evaluation of toxicity of PB-NEBP liposomes

Cell viability was assessed using the CCK8 kit (Beyotime, China) following the manufacturer's guidelines. Briefly, 5×10^3 HUVECs in 100 μL of induction medium was planted within 96-well plates, and processed by ranging concentrations of PB-NEBP Liposomes for 24h. Post incubation, 90 μL serum-free medium and 10 μL cck8 were supplemented into each well, following 1h 37°C incubation. Consequently, the product was detected at 450 nm under microplate reader.

For hemolysis evaluation, freshly collected blood from anesthetized mice, anticoagulated with Ethylene Diamine Tetraacetic Acid (EDTA), was sent for a series of meticulously orchestrated steps, inclusive of centrifugation, washing, and meticulous 10-fold dilution with PBS, to procure pristine RBCs. In the experimental setup, 200 μL of diverse solutions were introduced to 1 mL of RBCs, and incubated for a stipulated 4h period at room temperature. RBCs immersed in PBS functioned as the negative control, while those in water served as the positive control. Following incubation, supernatants were meticulously harvested through centrifugation, and the absorbance was quantified at 540 nm using a sophisticated microplate reader. Hemolysis percentage was computed via the formula: hemolysis % = (Sample group absorbance - PBS group absorbance) / (Water group absorbance - PBS group absorbance) × 100%.

To gauge the *in vivo* toxicity of PB-NEBP Liposomes, a cohort of 5 pregnant ICR mice received intravenous injections of 200 μL of PB-NEBP Liposomes solution (4mg/mL) at designated intervals (G14.5, G15.5, G16.5). Concurrently, a control group of 5 healthy mice received intravenous injections of saline. Retroorbital blood samples were collected for comprehensive hematology analysis on day G17.5.

For the assessment of postnatal viability and offspring growth, cesarean sections were meticulously performed on G17.5. Each fetus and placenta underwent individual weighing. Fetus specimens were preserved in a 95% ethanol solution and subjected to an intricate skeletal staining procedure involving Alcian blue and Alizarin red S for comprehensive skeletal examination. The major organs extracted from pregnant mice were systematically collected and subjected to HE staining, facilitating a detailed pathological analysis post-sacrifice.

QUANTIFICATION AND STATISTICAL ANALYSIS

All experiments were conducted at least 3 times. Statistical significance is reported in Figure Legends, and data are presented as mean ± SD. Statistical variances among the experimental cohorts were evaluated utilizing one-way ANOVA or T-test via GraphPad Prism software version 8.0 (*$p < 0.05$, **$p < 0.01$, ***$p < 0.001$, and ****$p < 0.0001$).